Numerical Investigation of Critical Range for the Occurrence of Secondary Peaks in the Nusselt Distribution Curve

Open Access

Siddique Mohammed Umair[1,*], Abdulrahman Alrobaian[2], Sher Afghan Khan[3], Marthande Gnanagonda Kashinath[4], Patil Rajesh[4]

[1] Mukesh Patel School of Technology Management and Engineering, Mumbai, Maharashtra, India
[2] Mechanical Engineering Dept., Qassim University, Buraidah, Saudi Arabia
[3] Mechanical Engineering Dept, Faculty of Engineering, International Islamic University Malaysia, Kuala Lumpur, Malaysia
[4] Mukesh Patel School of Technology Management and Engineering, Mumbai, India

ARTICLE INFO

ABSTRACT

The study of heat transfer augmentation in micro/nano scale and electronic packaging systems are some of the paramount areas of impending universe. In such systems the cooling of the hot heat sinks is generally achieved through the impingement of air jet. In order to study the characteristic of heat dissipation rate, variation of Nusselt number versus radial distance over the target surface is investigated. The magnitude of Nusselt Number is found to decrease gradually with increase in the radial distance away from the jet. The record of Nusselt magnitude over the radial distance is accomplished through computation using ANSYS CFX 14.5. A 2-D axis-symmetric model consisting of nozzle and target surface with discrete meshing is solved using an appropriate turbulence model, in order to develop the flow regime and record the necessary heat interactions. As far as the transition and intermediacy in flow structure at the target surface due to the unpredicted transport of shear stress is concerned, SST along with Gamma – Theta turbulence model is solved simultaneously in order to incorporate these phenomena.. The occurrence of such secondary peaks increases the heat transfer rate. Looking into the light of research area in determining the exact cause and the intervening range for the occurrence of such peaks, the current research focuses over the determination of the critical range within which the secondary peaks exists. This critical range comprises of multiple of jet to the target spacing and diameter-based Reynolds number and the corresponding critical range is between 2205 and 26, 46, 000. Not only that the velocity contour of the flow regime is mapped for the sets of parameters within the critical range. An empirical correlation for the area averaged Nusselt number terms of Reynolds number and jet to the target spacing being is proposed. This correlation improvises the calculation of the magnitude of area.

* *Corresponding author.*
E-mail address: u.i.siddiqui@gmail.com (Siddique Mohd Umair)

1. Introduction

Heat transfer augmentation using steady/pulse jet impinging on flat plate finds abundant applications in material processing industries, drying technologies and electronic packaging system. As far as the efficiency of these appliances is concerned, cooling rate due to impingement of air jet plays a bottom line role. Application of air jet impingement in cooling of microelectronic chips, material processing industries, design of heat sink, cooling of gas turbine blades and robotics application is the upcoming challenge of the impending universe. In this attempt the noisy components like fans and blowers can be replaced. Cooling of these appliances using air jet gives comparatively higher cooling rate as that achieved by conventional cooling practices. Generally, the rate of cooling is measured by calculating Nusselt number which represents the magnitude of convective heat transfer. As far as cooling of heat sink by impingement of air jet is concerned, proper calculation of area averaged and local Nusselt number becomes a challenging task when the distribution curve becomes non-uniform. This non-uniformity in Nusselt distribution curve arises due to the presences of secondary peaks. This unpredictable rise occurring in the far field area or in the stagnation region generally depends upon jet to the target spacing and impinging Reynolds number.

1.1 Literature Overview

The basic research for studying the convective heat transfer coefficient due to air jet impingement is mostly carried out experimentally. The common experimental setup used, basically consist of a target plate and an air impinging nozzle. Nozzle carries air at a specified Reynolds number and impinges it over the hot target surface. Thermocouples mounted over the plate enables the local temperature measurement. This is how the Nusselt number distribution curve is plotted over the radial distance on the target surface. However, it is observed that extensive research is carried out in the field of air jet impingement cooling mechanism by plotting local Nusselt number distribution curve over a flat plate and modified target surfaces.

El–Sheikh *et al.*, [1] compared the heat transfer coefficient for unpinned and pinned surface in presence of single and multi-jet by varying Reynolds number, jet to the target spacing and diameter of nozzle. The graphical justification showed the strong dependency of heat transfer coefficient on the air flow rate of impinging jet. 60% increment in heat transfer rate was obtained for pinned surface in presences of multi jet with that compared to unpinned ones. Also, the stagnant point Nusselt number was being correlated as $Nu = 3.361\ Re^{0.724}\ Pr^{0.4}\ (D_e/d)^{-0.689}\ (S/d)^{-0.10}$.

Garimella *et al.*, [2] further took an effort in determining the local heat transfer coefficient at different radial distances of pin fin surface by varying H/d and Reynolds number. Comparison was made between the multi jets impinging array of 9×1.59 mm and 4×3.18 mm with single jet. 20% increment in heat transfer coefficient for 4×3.18 mm over 9×1.59 mm was observed. The dominancy of multi jet in heat transfer coefficient observed was due to intermediate peaks in Nusselt distribution curve. These intermediate/secondary peaks seem to shift toward the centre because of which the Nusselt distribution curve becomes flattened. This happens with simultaneous increase in Reynolds number and decrease in jet to target spacing. Furthermore, the stagnant point Nusselt number in terms impinging and geometric parameter was correlated as $Nu_s = 0.161\ Re_s^{0.707}\ Pr^{0.4}\ (H/d)^{-0.104}$. On the other hand Yoshisaburo *et al.*, [3] determined the effect of jet to the target and inter jets spacing on heat transfer rate using thermochromic liquid crystal.

As far as impingement over a flat plate is concerned, extensive research is carried with wide range of impinging and geometric parameter in order to study the Nusselt distribution curve. Not

only that the use of multi jet in combination with flat plate has plenty studies. But calculation of area average Nusselt number over the surface and its significant effect due to the presences of secondary peak is yet too worked upon.

Lytle *et al.*, [4] performed experimental study for heat transfer distribution over a flat plate at low Z/d spacing, in order to capture the secondary peaks. At low Z/d spacing two peaks apart from that occurring at stagnation point was observed due to accelerated radial flow just exit to the tube.

The secondary peaks in Nusselt distribution curve was being justified due to the termination of flow within the length of potential core. On-behalf of this destroying of potential core, turbulence get induced inside and outside the stagnation region resulting in thinning of boundary layer. As a result of which secondary peaks occurs and heat transfer increases. Also, the local radial distances at which these peaks exist were examined in terms of Reynolds number. On the other hand Choo *et al.*, [5] experimentally determined the effect of pumping power on heat transfer distribution over a flat plate under steady air jet impingement. Experiments were performed at jet to the target spacing equals to one and less than one. A remarkable peak in Nusselt distribution curve far away from stagnation point at r/d = 0.125 with impinging Reynolds number of 5100 was observed.

The above research was conducted on experimental setup in which the effort and time required are enormous. Further to demonstrate huge sets of experimental reading at different varying parameter, experimental analysis becomes a less powerful tool. Hence the need arises for solving the heat transfer augmentation problem via numerical analysis.

Huang *et al.*, [6] on the other hand studied heat transfer distribution over a flat plate by impinging the mixture of water and particles of aluminium oxide. Numerical analysis was carried at different concentration of nanofluids, Reynolds number and Z/d. The results of simulation revel the strong dependence of concentration ratio of nanofluids on local heat transfer coefficient. In order to consider the turbulence and mixing regime, Huang *et al.*, [6] selected SST turbulent model. Furthermore, secondary peaks in the Nusselt distribution curve was observed at H/d = 2 and Reynolds number of 2000 with the magnitude being more prominent at higher concentration. The studied lagged in justifying the physical significance behind the occurring of these peaks.

Gorji *et al.*, [7] examined ten types of eddy viscosity turbulence models in predicting the flow behaviour for ramp up flow. Three ramps up flow with different acceleration were chosen for experimentation. Turbulent shear stress transport was captured with respect to the change in flow rate while the delay in capturing of dynamic turbulent shear stress by the current computational model was observed. Hence the results of different thermo physical parameters in transition region seem to be inaccurately plotted. Whereas gamma theta model proposed by Langtry *et al.,* [8] proves to capture these delays far accurately. This is achieved by invoking an intermediary term whose value ranges from zero to unity inside the boundary layer. Malan *et al.*, [9] completely calibrated the gamma theta model by coupling it with SST turbulence model. This calibration work was carried out by numerically analysing the flat plate and air foils at different flow rate. As far the capability of this coupled (SST + Gamma – Theta) turbulence model in commercial computing software is concerned, it was observed to capture the transition flow regime and corresponding heat interaction far accurately.

Hence the use of Gamma Theta model becomes necessary as far as transition in the flow regime is concerned. Also, it controls in the arena of transition region based on predefined onset transition Reynolds number. It is therefore recommended to use SST transition model along with Gamma – Theta in order to capture the Nusselt distribution curve accurately. This also proves significant in capturing secondary peaks.

Angioletti *et al.*, [10] visualized the flow contour by laterally impinging air jet over a flat plate with the help of PIV. In this study k - ε, k - ω and SST turbulence models was examined for flow

analysis and results for velocity contour were plotted. Looking into the velocity contour it was observed that the flow of air jet before striking the plate was found to spread. This happen due to entrainment of fresh air which cannot be noticed in PIV plots. This effect was found to be well captured by SST turbulence model which gave the most accurate prediction of the realizable flow field. Also, stagnant point was accurately seen to be configured. On the other hand Antar Alenezi *et al*., [11] compared k - ε, k - ω and SST turbulence models for analysing the flow development inside a narrow trench at Mach number of 1. The study incorporated the computation using commercial software CFX. On behalf of the computation SST turbulence model showed quite accurate development of flow field and thermal regions.

Hence it is concluded that the score of research around secondary peaks formation, its physical reasoning and the promising condition for its occurrence is very less. Not only that, a dedicated empirical relation for calculating area averaged Nusselt number in presences of secondary peak lags.

No doubt Katti *et al*., [12] came forward in this issue and extensively plotted local Nusselt distribution curve over the flat plate at lower jet to the target spacing. Here the impingement of air was carried out at Reynolds number ranging from 12,000 to 28,000 and Z/d from 0.5 to 8. Katti *et al*., [12] observed the secondary peaks for the first time at Z/d = 0.5 and concluded the existence transition in flow regime at target surface to be responsible. Furthermore, the ranging condition for existences of secondary peaks in terms of Z/d and Reynolds number remains incomplete. Also, the condition signifying the occurrence of secondary peak in terms of jet to the target spacing and impinging Reynolds number remains vacant.

Abubakar and Sidik [17] determined the effect of magnetic field on nano fluids, the result of the present work reveal that increasing the volume fractions provide a better heat transfer enhancement and increasing the Reynolds number caused an increase in volume fraction. Qin *et al.,* [18] determined the effect of fins height on heat transfer rate.The study found that heat transfer coefficient increases as the temperature difference between heat sink and ambient increases. Abubakar *et al.,* [17] studied the effect of laminar flow behavior in microchannels. Therectangular microchannel with hydraulic diameter of 86 μm and length of 10mm under the boundary condition of constant heat flux and uniform inlet velocity was set on the analysis. Results of this work using Fe_3O_4-H_2O_4 as coolant were expected to give higher efficiency of heat transfer in microchannel heat sink in comparison to pure water. On the other hand Jamil *et al.,* [19] correctly predicted the development of flow profile using different turbulence model in CFX solver.

1.2 Objective of Present Work

It is observed that extensive research is carried out in determining the empirical correlation for area averaged and local Nusselt number at lower jet to the target spacing. Also, there exists no evidence of specific correlation used to determine the magnitude of Nusselt number in presences of secondary peak. Looking into the tangible gap in the research area of secondary peaks, it can be concluded that the promising condition for existence of secondary peaks in terms of impinging parameter is necessary to be constructed.

Furthermore, an empirical correlation for area averaged and local Nusselt number in terms of various impinging and geometric parameter needs to be developed. This correlation can be used in calculating the magnitude of Nusselt number in presences of secondary peaks analytically. Not only that, the present work takes an additional effort in plotting the velocity contours at critical sets of parameters. On behalf of which, physical understanding of the existences and vanishing point of secondary can be visualized. This is achieved by solving the optimized geometry of current problem ANSYS CFX 14.5.

2. Experimental Setup

In order to plan the intervention period and to develop the necessary correlation for which the secondary peaks in the Nusselt Distribution curve occurs; measurement of temperature at various location of target plate becomes mandatory. The current setup avails the variation in impinging Reynolds number, jet to the target spacing, heat input and the type of target surface used for impingement. During the initial periods of impingement of air on target surface, the temperature of target surface decreases with time. Readings of thermocouples are recorded at steady state.

2.1 Apparatus

The basic experimental setup to measure heat transfer through aluminium flat surface (100mm $\times$ 100mm) consists of inlet blower of capacity 0.05 m^3/s which pumps the fresh atmospheric air into a cylindrical chamber called air plenum. Also, with the help of rotating handle mounted on threaded shaft which is further riveted to air plenum, jet to the target spacing can be adjusted as shown in Figure 1. Electric heater mounted on the bottom side of the surface (Heat sink) provides constant heat throughout the surface body. Data Acquisition system (DAQ) ensures the recording of instantaneous and local temperature of heat sink. This is achieved with the help of four thermocouples mounted on the diagonal line joining the corners of heat sink at equal radial distances away from the centre, as seen in Figure 2.
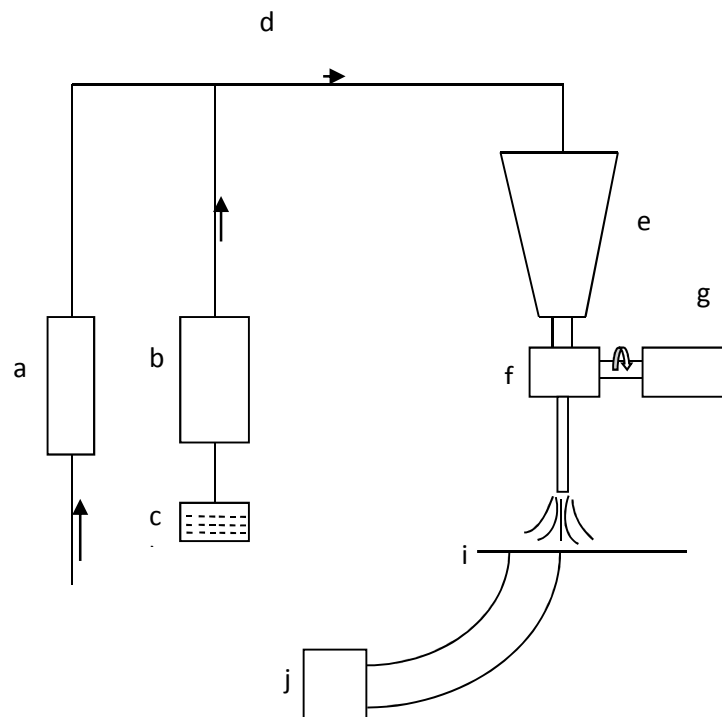
Fig. 1. Shows schematic layout of test setup. a) air compressor, b) fog machine, c) fog liquid, d) air pipe, e) Plenum, f) Pulsating valve, g) motor, h) nozzle, i) flat plate, j) Data logger system.
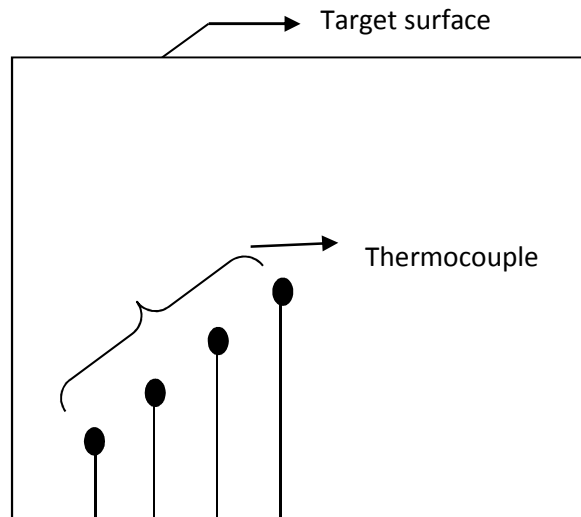
Fig. 2. Positions of thermocouple on base plate

2.2 Calibration of Experimental Setup

In order to confirm the accuracy of heat transfer measurement, the present work is being calibrated against the following experimental results: Persoons *et al.*, [13] in which experiments are performed at H/d = 1, 6 and 13mm as a diameter of nozzle. Alimohammadi *et al.*, [14] Jet to the target spacing was equal to the diameter of nozzle and Chougle *et al.*, [15] in which Computational analysis for heat transfer coefficient distribution over a 60×60mm flat plate at H/d = 6 with 5mm as diameter of nozzle is carried out. considered Prandtl number as an additional non-dimensionless number in order to calibrate his own results. But the present work incorporates Nusselt number, Reynolds number and H/d as a keystone parameter in order to calibrate the magnitude of area average Nusselt number. Figure 3 shows the variation of Nusselt number with Reynolds number for previous works and present study.
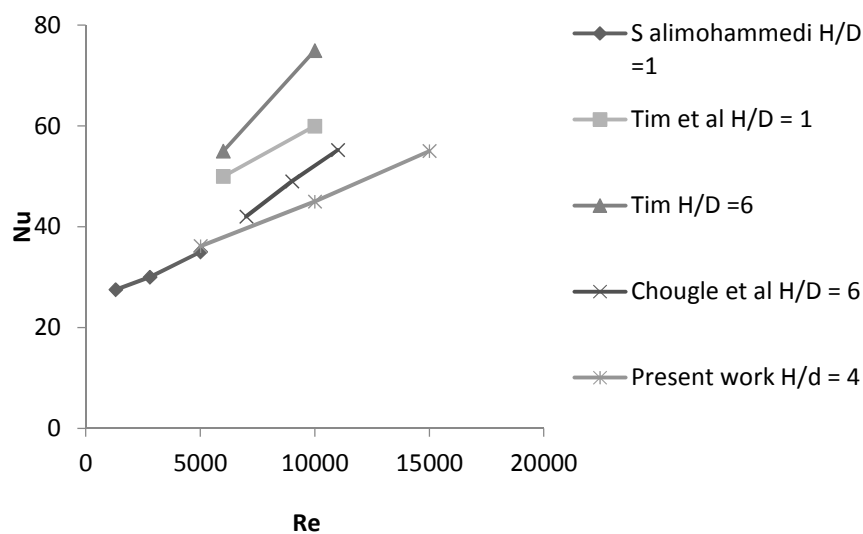
Fig. 3. Shows the comparative results of previous research works

3. Methodology

3.1 Heat Transfer Measurement Due to Steady Jet

Rate of Cooling for flat aluminium plate is measured with the help of forced convective heat transfer coefficient at steady state as shown in Equation (1)

$$h = \frac{Q}{A \times (T_b - T_a)} \tag{1}$$

T_b is base plate temperature measured at steady state. Nusselt number is the non-dimensional parameter which measures the ratio of the magnitude of heat convected due to impinging air jet to the heat conducted as shown n Equation (2).

$$Nu = h \times \frac{d}{k_a} \tag{2}$$

The current work defines the Nusselt number considering diameter of nozzle as its characteristic length.

3.2 Numerical Method for Heat Transfer Measurement

As far as the time and energy for performing the experiment is concerned, it seems to be consuming a huge time in order to give the results for temperature distribution over the plate. Since the temperature profile consumes a great time to become constant. In order to compensate for this physical time and energy, numerical simulations are being suggested and are being carried out in the present work.

The numerical method commands the continuity, momentum and energy equation to be solved simultaneously in order to develop the flow regime and plot the corresponding heat interaction. This is achieved by simulating the geometry in commercial simulating software ANSYS CFX 14.5. Taking into consideration the computational time and cost a 2-D axis symmetric model was developed as seen in Figure 4. In order to solve the flow field, the present computation methodology calls SST transition model along with Gamm-Theta models. This is done in order to ensure the accurate development of flow regime and its corresponding heat transfer rate. This set of turbulence model proves to be far accurate in capturing the heat transfer rate during the period of intermediacy and separation in flow regime.

3.2.1 Numerical method for heat transfer measurement

As far as the time and energy for performing the experiment is concerned, it seems to be consuming a huge time in order to give the results for temperature distribution over the plate. Since the temperature profile consumes a great time to become constant. In order to compensate for this physical time and energy, numerical simulations are being suggested and are being carried out in the present work.

The numerical method commands the continuity, momentum and energy equation to be solved simultaneously in order to develop the flow regime and plot the corresponding heat interaction. This is achieved by simulating the geometry in commercial simulating software ANSYS CFX 14.5. Taking into consideration the computational time and cost a 2-D axis symmetric model was developed as seen in Figure 4. In order to solve the flow field, the present computation methodology calls SST transition model along with Gamm-Theta models. This is done in order to

ensure the accurate development of flow regime and its corresponding heat transfer rate. This set of turbulence model proves to be far accurate in capturing the heat transfer rate during the period of intermediary and separation in flow regime.

Further the designed model is imported into mesh deign modeler for the purpose of meshing. This is done under the same computation tree. Generally, tetrahedron meshing with flexible growth rate and edge size is performed in order to discrete the computational domain. During the process of meshing, the edges containing air jet and base plate are intentionally divided into a greater number of divisions as compared to rest. This increases the grid density and population in the region containing air jet and base plate.
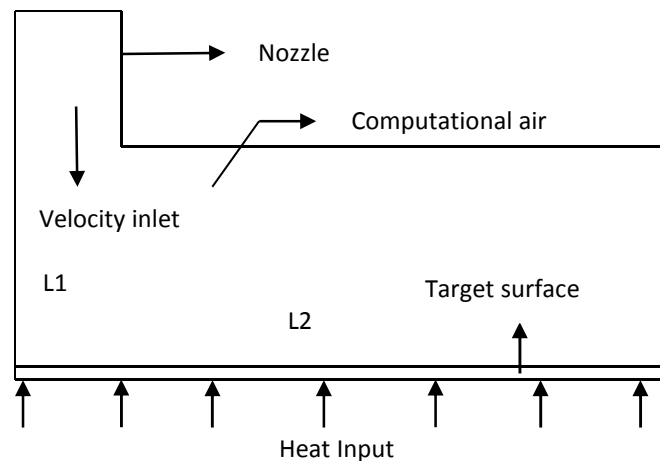
Fig. 4. Schematic layout of 2-D axis symmetric computational geometry

3.2.2 Turbulence model

Looking into the magnitude of impinging Reynolds number it seems that the flow is highly turbulent in near wall region of flat plate and remains confined just at the exit of nozzle. Due to this complication, K -ε and *K- ω* turbulence model does not give an accurate temperature profile over the plate, while on the other hand SST transition model which considers both effects simultaneously confirms the accuracy. Furthermore, in order to capture the distinct results of heat transfer augmentation where intermediary and onset transition of Reynolds number in the flow regime occurs, *Gamma – theta* transition models are coupled along with modified SST model to arrest secondary peaks and provides gradual decreasing Nusselt profile. Alimohammadi *et al*., [16] performed model dependences test in which the temperature profile for *K* -ε and *K- ω* models were found to be almost independent of radial distance. On the other hand, SST turbulence model along with Gamma – *theta* manifests the strong dependency of Nusselt number over the radial distance.

3.2.3 Boundary conditions

The present axis symmetric geometry as shows in Figure 4 is solved in ANSYS CFX 14.5. Overall the computational domain is classified into two categories, fluid and solid (plate) domain. The exit wall of the nozzle is provided with velocity inlet with a turbulence intensity of 1-3%, as justified by Alimohammedi *et al*., [16]. On the other hand, the opening of domain in atmosphere is set to zero-gauge pressure and atmospheric temperature. Also, a constant heat flux input is provided at the

bottom of the plate to ensure uniform and constant heating. Four to five points on the surface of the plate are being monitored during computation to see the temperature variation across the plate.

3.2.4 Grid dependences test

In order to compare the dependency of Nusselt distribution curve on grid size, area averaged Nusselt number is calculated for different grid sizes. The density of grid near jet region in air domain and on the surface of plate is kept intentionally more as compared to that in far field areas of air domain as shown in Figure 5. Of all the edges present, the edge containing (L1, L2) jet to the target spacing and base length of the target surface is subjected to variation in the number of divisions. On behalf of this, different values of area averaged Nusselt number are recorded for different grid sizes, as shown in Table 1 Number of divisions on the edges L1 and L2 are varied from 300 to 550 and 125 to 400 respectively. Comparison of area averaged Nusselt number with its preceding value and experimental value define the most accurate grid size. This corresponding mesh consists of 550×400 numbers of divisions on edges L1 and L2 respectively. If the computational model is subjected to change in jet to target spacing and base length, it is recommended to change the number of divisions by the appropriate multiples. However, the current grid dependence test was carried out at $Z/d = 4$ with the base length of 50 mm.
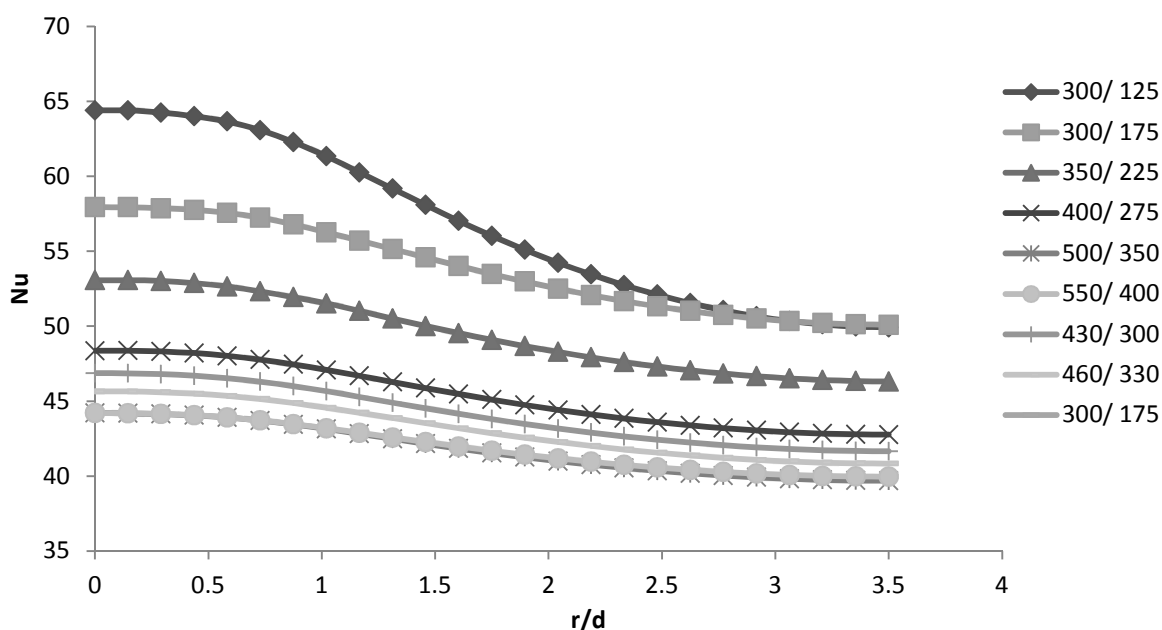
Fig. 5. Shows the Nusselt Distribution curve for number of divisions over edges L1 & L2

3.2.5 Model dependence test

As far as the flow regime and transition of flow after impingement is concerned, the commercial flow turbulence model available in the solver is not capable of predicting the Nusselt distribution accurately. The flow structure over the target surface after impingement consist of a stagnation region (0 < r/d <1.0), transition region (1.0 < r/d < 2.5) and wall jet region (r/d>2.5) as being described. Hence there is a need of turbulence model which accurately records the temperature profile in the arena of near jet and wall jet region simultaneously.

Table 1 shows a comparison between the successive computed area averages Nusselt Number. Not only that the computed value is also compared with its corresponding experimental value. It is seen from Table 1 that mesh size containing 550 number of divisions of edge L1 and 400 numbers of divisions on edge L2 resembles the least deviation from its preceding value.

Table 1
Comparison of area average Nusselt number at different grid size

Edge sizing		Computed Nu_{avg}	Percentage Deviation with preceding value	Percentage deviation with experimental value
Base (L1)	Jet to target spacing (L2)			
300	125	59.76	--	30.36%
300	175	53.83	10%	22.69%
350	225	49.46	8.1%	15.86%
400	275	45.38	8.2%	8.3%
430	300	44.08	2.87%	5.6%
460	330	43.09	2.23%	3.44%
500	350	42.48	1.41%	2.05%
550	400	41.92	1.32%	0.74%

K-ε model is capable of well predicting the Nusselt distribution in stagnation region while K-ω model predicts well in wall jet region. On the other hand, SST model incorporates both the regions of flow regime and predicts accurate heat transfer dissipation as compared to K- ε and K-ω turbulence model. But the existence of transition, intermediary and varying onset transition momentum-based Reynolds number in the flow structure either promoted or degrades the Nusselt number. This phenomenon is not considered in any of the commercial CFX or FLUENT model. In order to consider the effect of heat transfer due the presence intermediary and transition flow, Langtry *et al.*, [9] proposed a transition models (Gamma – theta) which can be coupled to SST model in CFX solver. The benefit of this model lies in the accurate prediction of Nusselt number in the intervention period of intermediary and transition. Figure 6 shows a variation of local Nusselt number with respect to radial distance for different turbulence model.
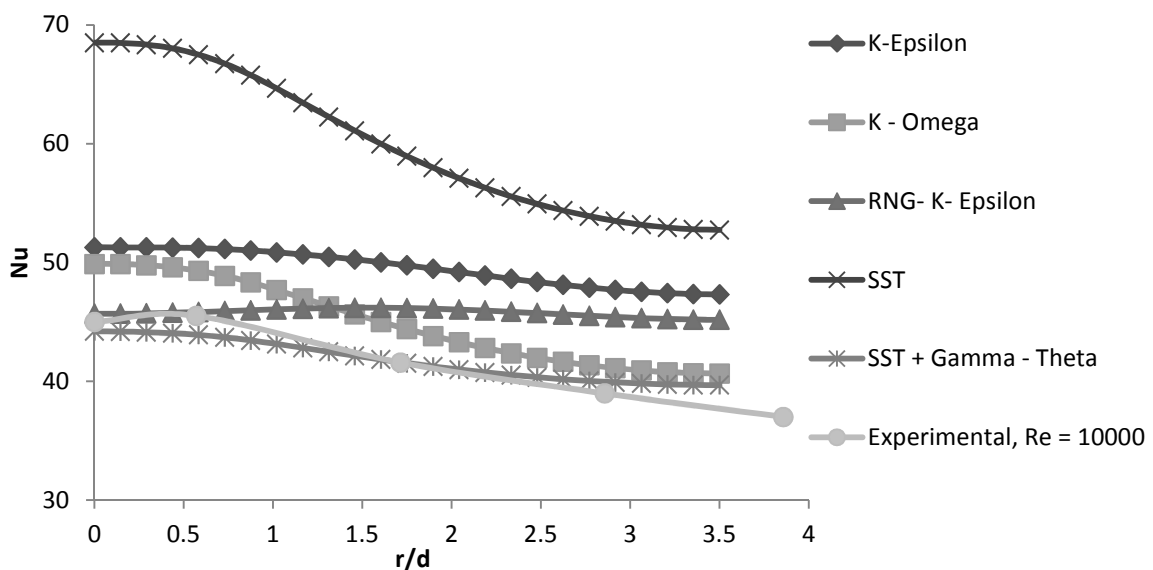
Fig. 6. Dependency of Nusselt distribution curve on turbulence model

Hence it can be concluded that SST transition model coupled with Gamma-Theta gives the most accurate prediction of heat transfer rate, by considering the magnitude of intermediary and

controlling its location. This is achieved by continuous calculation of vortices-based Reynolds number which needs to be served as an input to Gamma – theta model. On behalf of this the solver needs to solve three equations (SST + Gamma – Theta) simultaneously to most accurately predict the Nusselt distribution curve.

It can be seen from Table 2, SST along with Gamma – Theta transition model shows a very close resemblance with experimental value. On the other hand, K-Epsilon, K-Omega, SST and RNG-K-Epsilon are not capable of predicting that accurate. An error of 0.406% can be observed between experimental and computed value with use of SST along with two transition models.

Table 2
Comparison of average Nusselt number computed through different turbulence model

Turbulence model.	Results for area averaged Nusselt number.		Percentage Deviation.
--	Computational	Experimental	--
k – epsilon	49.5346	41.612	16%
k - omega	44.92596	41.612	7.37%
RNG-k-epsilon	45.78688	41.612	9.12%
SST	59.96172	41.612	30.6%
SST + Gamma-Theta	41.78259	41.612	0.406%

3.3 Parameter Specification

As far as the variation in geometric and injection parameter is concerned, velocity of impingement and jet to the target spacing are varied over the wide range as shown in Table 3.

Table 3
Range of various injection and geometric parameter

Parameters	Range
Velocity of impinging jet	$10 - 350$ m/s
Z/d	$1 - 30$
Diameter of nozzle	7.35 mm
Area of base plate	100×100 mm2
Heat input	15 Watts

4. Results

The local rise in Nusselt distribution curve is observed due to the presences of secondary peaks. These peaks are localized in stagnant and transition region. The intervening period for their occurrence solely depends upon the impinging Reynolds number and jet to the target spacing. The present work is inclined towards the determination of this intervening period, during which the secondary peaks occurs. In order to determine this critical range, numerical results for local Nusselt number over the flat plate are being evaluated at
i) Fixed jet to the target spacing with varying Reynolds number.
ii) Fixed Reynolds number with varying jet to the target spacing.
As observed from the previous literature, there exists a critical range comprising of the sets of parameters within which secondary peaks appears in the Nusselt distribution curve. These sets of

parameters generally comprise of the density, viscosity and velocity of the impinging fluid. On the other hand, jet to the target spacing and diameter of nozzle are the geometric parameter.

Above all the lower limit of this critical range is determined at fixed jet to the target spacing and by decreasing the impinging Reynolds number (Figure 7). While the upper limit is determined by increasing jet to the target spacing at fixed Reynolds number (Figure 8). Since the impinging velocity and jet to the target spacing carries an inverse variation, hence their multiple lands to a constant, Equation (3). This constant represents a modified Reynolds number carrying jet to the target spacing as a characteristic length.

$$\frac{Z}{d} \times Re_d = Re_z \qquad (3)$$

The current research considers the jet to target spacing based Reynolds number as the critical non-dimensional number in representing the critical range. This modified Reynolds number (Re_z) is used for setting the range in which the appearances of secondary peaks in Nusselt distribution curve are liable.

4.1 Nusselt Distribution over the Target Surface at Fixed Jet to the Target Spacing and Varying Reynolds Number

In order to capture the lower limit where origination of secondary peaks occurs, the 2-D axis-symmetric model is computed at different inlet velocities, ranging from 50 – 350 m/s. While the jet to the target spacing is maintain constant. Figure 7 shows the origination of secondary peak in the Nusselt distribution curve occurring at the inlet velocity of 30m/s. Above this critical value with constant jet to the target spacing the appearance of secondary peaks becomes more remarkable and localized. Hence the impingement velocity of 30m/s is considered as a critical value in deciding the origination of secondary peaks. The corresponding jet to the target spacing based Reynolds number (Re_z) approximates to 44000.
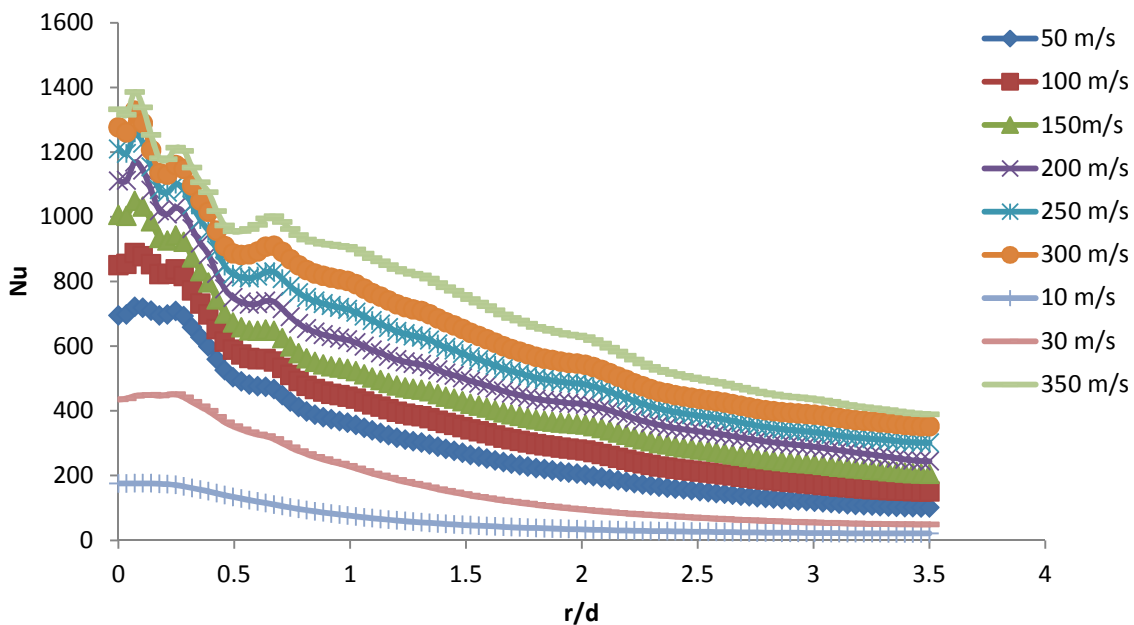
Fig. 7. Variation of Nusselt Number against radial distance at different velocity and constant jet to target spacing

4.2 Nusselt Distribution over the Target Surface at Fixed Reynolds Number and Varying Jet to the Target Spacing

The diminishing point for the appearance of secondary peak is investigated at fixed impinging velocity and increasing jet to the target spacing. No doubt the origination is computed at fixed spacing and increasing velocity. Figure 8 shows the plot of Nusselt distribution curve at constant velocity of 200 m/s and varying jet to the target spacing. The variation in the spacing ranges from 5 – 30 times the diameter of nozzle. As seen from Figure 8, the secondary peak at higher spacing become small and diminishes at a critical instant. In the current research this diminishing point is seen at jet to the target spacing of 30 times the diameter of the nozzle. The corresponding jet to the target spacing based Reynolds number is approximated to 26, 46,000.

Looking into the origination and diminishing point in terms of jet to the target spacing based Reynolds number, the critical range for the appearance of secondary peaks in Nusselt distribution curve can be concluded by Equation (4).

$$2205 \leq Re_z \leq 26,46,000. \tag{4}$$
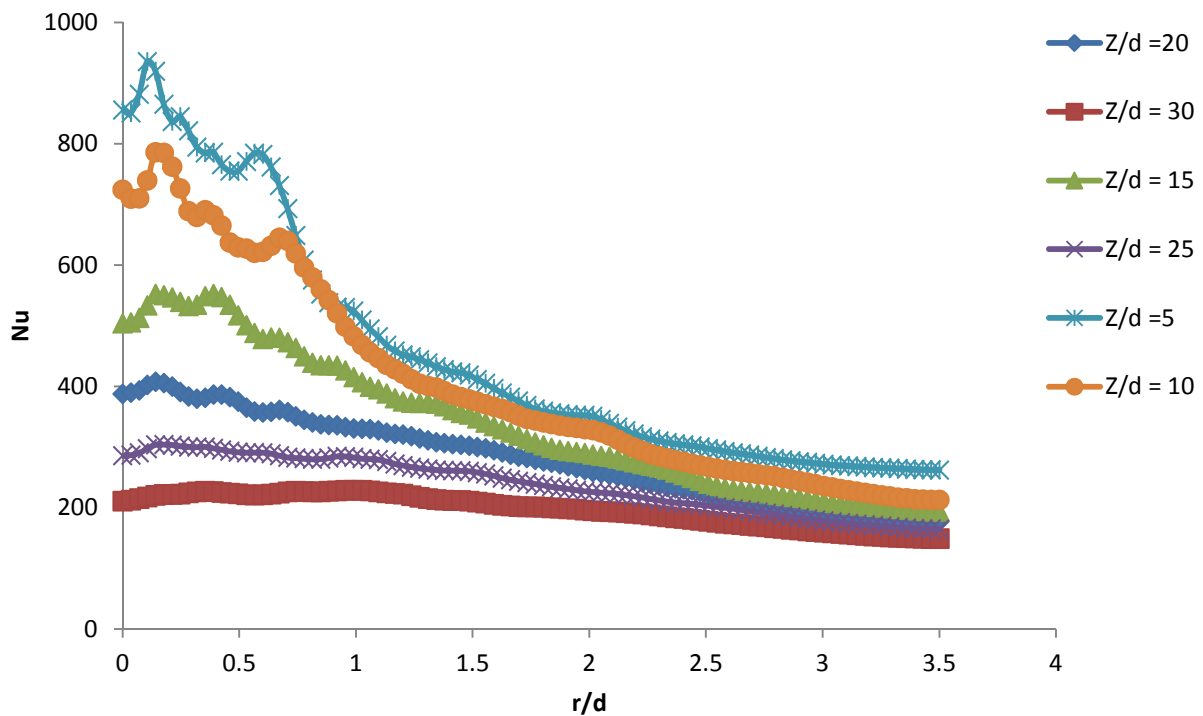
Fig. 8. Variation of Nusselt number against the radial distance at different jet to the target spacing and fixed impinging velocity

4.3 Physical Justification

It is clear from the Equation (4) that the origination and diminishing point occurs at jet to the target spacing based Reynolds number of 2,205 and 26, 46, 000 respectively. However, the secret behind the occurrence of secondary peaks is the transition occurring in the flow regime over the target surface. To visualize this transition layer, velocity contours are mapped at different jet to the target spacing based Reynolds number. Four different Velocity contours are mapped of which the

first two (Figure 9 and Figure 10) demonstrates the origination of secondary peaks. While Figure 11 and Figure 12 justifies the intermediate and vanishing period of the secondary peaks.

The maps of velocity contour show the presences of stretched region corresponding to which secondary peaks in Nusselt distribution curve occurs. This stretched layer comprises of cross velocity almost equivalent to that present in potential core. Due to increase in cross velocity at intermediate position over the target surface, heat transfer coefficient increases for a small instance and again gradually decreases. This increase in heat transfer coefficient for a very small instant due to the presences of transition region over the plate gives rise to secondary peaks in Nusselt distribution curve. Within the critical range as mentioned in Equation (4), the radial momentum of the flowing fluid increases above the theoretical value due to the slippage of fluid molecule occurring over the stagnation region.
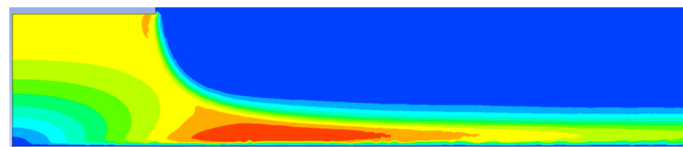
Fig. 9. Velocity contour at Re_z = 6, 615
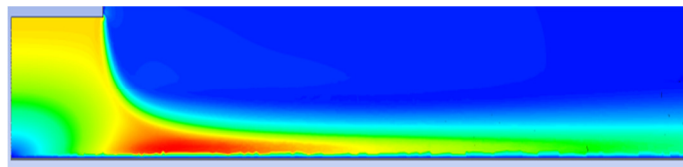
Fig. 10. Velocity contour at Re_z = 11, 025
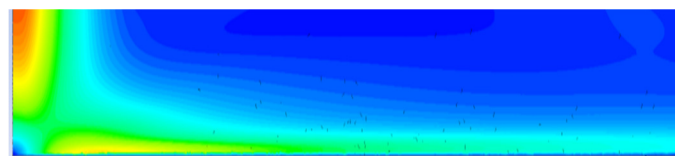
Fig. 11. Velocity contour at Re_z = 4, 41, 000

Fig. 12. Velocity contour at Re_z = 26, 46, 000

4.4 Correlation Ship Development

Empirical correlation for area averaged and local Nusselt number is already proposed by Alimohammedi *et al.,* [16]. The current work takes an additional effort in building up an empirical correlation dedicated towards the calculation of area average Nusselt number in presences of secondary peaks. The correlation enables the accurate determination of area averaged Nusselt number in terms of jet to the target spacing based Reynolds number.

Considering the limitation over the magnitude of least square coefficient, the correlation carries two divisions: origination and diminishing. Figure 13 shows the dependency of Re_z on area average Nusselt number and Equation (5) represents the possible correlation between them. This correlation is applicable only in the range of originating state of secondary peaks.
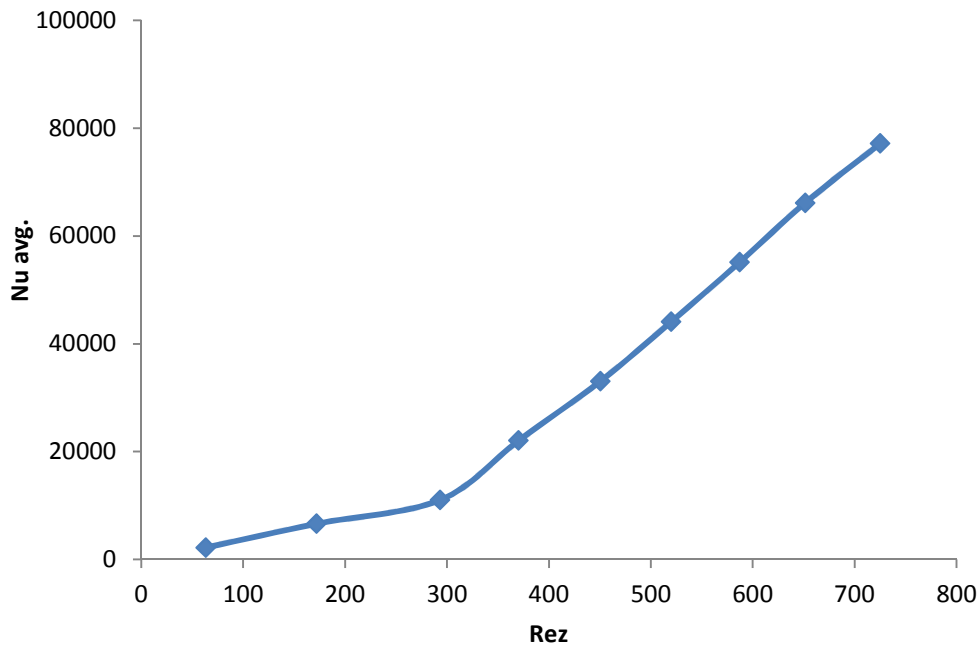
Fig. 13. Variation of area average Nusselt number with jet to the target spacing based Reynolds number in the originating state of secondary peaks

$$Nu = 0.7801 \times Re_z{}^{0.641} \quad (R^2 = 0.96) \tag{5}$$

On the other hand Figure 14 shows the dependency of Re_z on area average Nusselt number. While Equation (6) represents the correlation for area average Nusselt number in the diminishing state of secondary peaks.
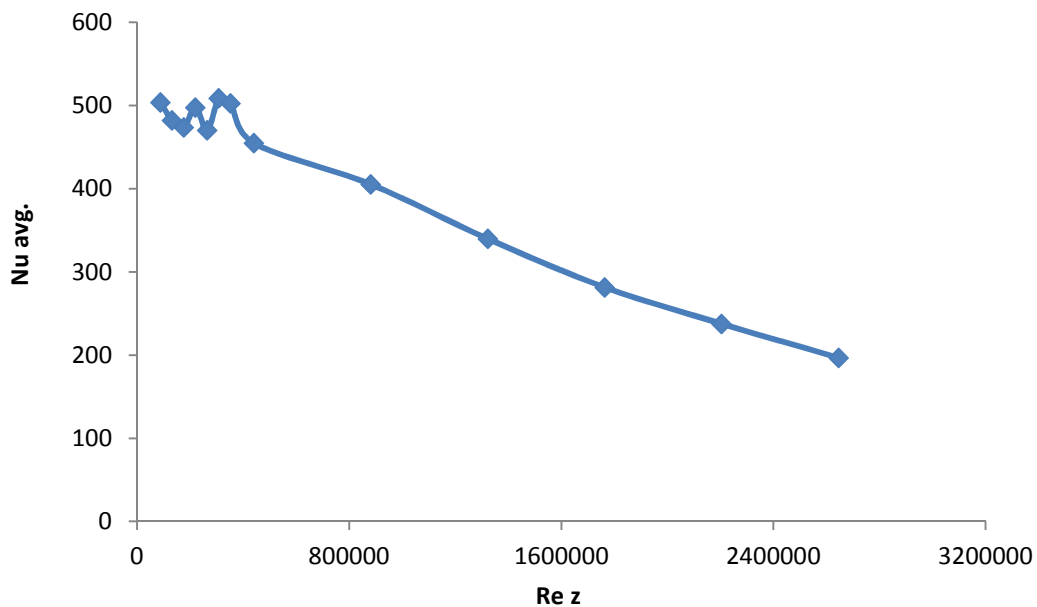
Fig. 14. Variation of area average Nusselt number with jet to the target spacing based Reynolds number in the diminishing state of secondary peaks

$$Nu = 57.51 \times Re_z{}^{-0.2562} \quad (R^2 = 0.89) \tag{6}$$

5. Conclusions

Hence the appearance of secondary peaks can be concluded to exist between 2, 205 to 26, 46, 000 of jet to the target spacing based Reynolds number. As seen from Figure 9-12 the transition region occurring just adjacent to the stagnation region is responsible for such abnormal rise in the Nusselt distribution curve. This transition region gets stretched at the cost of it lateral thickness as jet to the target spacing based Reynolds number approaches toward the upper limit. This stretch is observed to be maximum at a value of jet to the target spacing based Reynolds number. At this impingement condition, area average Nusselt number is observed to be superior. Now as jet to the target spacing based Reynolds number shifts away from this critical value and moves towards the upper limit, area average Nusselt number is found to decrease gradually. This signifies the diminishing state of transition skin where it starts shrinking at the cost of increasing lateral width. The diminishing state of this transition skin is achieved by successive transformation in to low velocity regions.

Above all there exist a instant in the critical range where heat transfer rate is maximum. It can be concluded from the current research that this instant lies in the range of $1, 76, 400 \leq Re_z \leq 2, 20, 5001$.

References

[1]   El–Sheikh, Hani A, and Suresh V Garimella. "Heat Transfer from Pin – Fin Heat Sinks under Multiple Impinging Jets." *IEEE Transaction on Advance Packaging* 23, no. 1 (2000): 113–19.
[2]   Garimella, Suresh V, and Vincent P Schroeder. "Local Heat Transfer Distributions in Confined Multiple Air Jet Impingement." *Journal of Electronic Packaging* 123 (2000): 165–72.
[3]   Yoshisaburo, Yamane, Yoshiyasu Ichikawa, Makoto Yamamoto, and Shinji Honami. "Effect of Injection Parameters on Jet Array Impingement Heat Transfer." *International Journal of Gas Turbine* 4, no. 1 (2012): 27–34.
[4]   Lytle, D, and B W Webb. "Air Jet Impingement Heat Transfer at Low Nozzle – Plate Spacing." *International Journal of Heat Mass Transfer* 37, no. 12 (1994): 1687–1697.
[5]   Choo, Kyo Sung, and Sung Jin Kim. "Heat Transfer Characteristics of Impinging Air Jets under a Fixed Pumping Power Condition." *International Journal of Heat and Mass Transfer* 53, no. 1–3 (2010): 320–26.
[6]   Huang, Jun-Bo, and Jiin-Yuh Jang. "Numerical Study of a Confined Axisymmetric Jet Impingement Heat Transfer with Nanofluids." *Engineering* 05, no. 01 (2013): 69–74.
[7]   Gorji, S., M Seddighi, C Ariyaratne, A E Vardy, T O'Donoghue, and D Pokrajac S He. "A Comparative Study of Turbulence Models in Transient Channel Flow." *Computer & Fluids* 89 (2014): 111–23.
[8]   Langtry, Robin B, and Florian R Menter. "Correlation – Based Transition Modelling for Unstructured Parallelized Computational Fluid Dynamics Codes." *AIAA Journal* 47, no. 12 (2009): 2894–2906.
[9]   Malan, Paul, Keerati Suluksna, and Ekachai Juntasaro. "Calibrating the gamma-Re_theta transition model for commercial CFD." In *47th AIAA Aerospace Sciences Meeting Including The New Horizons Forum and Aerospace Exposition*, p. 1142. 2009.
[10]   Angioletti, M, E Nino, and G Ruocco. "CFD Turbulent Modelling of Jet Impingement and Its Validation by Particle Image Velocimetry and Mass Transfer Measurements." *International Journal of Thermal Science* 44 (2005): 349–56.
[11]   Alenezi, A, J Teixeria, and A Addali. "Numerical Analysis of Heat Transfer Characteristic of an Orthogonal and Obliquely Impinging Air Jet on Flat Plate." In *Proceedings of World Congress on Engineering II*, 2015.
[12]   Katti, Vadiraj, and S V Prabhu. "Experimental Study and Theoretical Analysis of Local Heat Transfer Distribution between Smooth Flat Surface and Impinging Air Jet from a Circular Straight Pipe Nozzle." *International Journal of Heat and Mass Transfer* 51 (2007): 17–18.
[13]   Persoons, Tim, Kuanysh Balgazin, Karl Brown, and Darin B. Murray. "Scaling of Convective Heat Transfer Enhancement Due to Flow Pulsation in an Axisymmetric Impinging Jet." *ASME Journal of Heat Transfer* 135 (2013): 1–10.
[14]   Alimohammadi, Sajad, Darina B. Murray, and Tim Persoons. "Experimental Validation of a Computational Fluid Dynamics Methodology for Transitional Flow Heat Transfer Characteristics of a Steady Impinging Jet." *Journal of Heat Transfer* 136, no. 9 (2014): 091703.

[15] Chougle, N K, G V Parishwas, and C M Sewatkar. "Numerical Analysis of Pin Fin Heat Sink with a Single and Multi-Air Jet Impingement Condition." *International Journal of Engineering and Innovative Technology* 1, no. 3 (2012): 44–50.

[16] Alimohammedi, S, P Dinnen, T Persoons, and D B Murray. "Thermal Management Using Pulsating Jet Cooling Technology." *Journal of Physics Conference Series* 52, no. 5 (2014): 1–10.

[17] Abubakar, S. B., and NA Che Sidik. "Numerical prediction of laminar nanofluid flow in rectangular microchannel heat sink." *J. Adv. Res. Fluid Mech. Therm. Sci.* 7, no. 1 (2015): 29-38.

[18] Qin, Yap Zi, Amer Nordin Darus, Che Sidik, and Nor Azwadi. *Numerical analysis on natural convection heat transfer of a heat sink with cylindrical pin fin*. Vol. 695. Trans Tech Publications, 2015.

[19] Jamil, M.M., Adamu, M.I., Ibrahim, T.R. and Hashim, G.A., 2015. "Numerical Study of Separation Length of Flow through Rectangular Channel with Baffle Plates." *Journal of Advanced Research Design* 7, no. 1 (2015): 19-33.